

## Transport by single and few electrons in GaAs mesoscopic structures

D.H. Cobden, A.S. Dzurak, M. Field, C.G. Smith,  
A.K. Savchenko, M. Pepper, D.A. Ritchie, J.E.F. Frost,  
G.A.C. Jones and D.G. Hasko

*Cavendish Laboratory, Madingley Road, Cambridge CB3 0HE, UK*

A brief review is presented on some of the consequences of single electron transport in GaAs structures. Particular topics considered include noise and fluctuations in the ballistic regime where the quantised conductance imposes a limit on the magnitude of the random telegraphic signals and the consequences of single traps changing occupancy can be clearly observed. Results are also presented on the non-invasive detection of the Coulomb blockade and factors determining transport in the conductance minima are discussed. Thermo-electric effects in the blockade regime are discussed as these are complementary to studies of electrical transport and show that the thermopower oscillates about zero with a period corresponding to the removal of a single electron.

### 1. Introduction

An interesting aspect of transport in small structures is the quantisation of the one dimensional resistance when electron transport is ballistic. Here the conductance is given by  $\sigma = (2e^2/h)i$ , where  $i$  is the number of one dimensional subbands and the factor of 2 arises from the spin degeneracy which can be lifted by a parallel magnetic field [1,2]. Increasing the voltage which drives the current through the device lifts the degeneracy between  $+k$  and  $-k$  states and results in a further quantisation in units of  $e^2/h$  for a spin degeneracy of 2 or  $e^2/2h$  when the spin degeneracy is lifted [3]. These effects are now well understood and a considerable literature exists; here we present more recent results in mesoscopic physics.

The most versatile structure for the investigation of these effects is the AlGaAs–GaAs high mobility heterojunction where the conducting channel is defined by applying a voltage to a split gate. As the electron gas is defined by a smooth electric field so the high mobility is retained. The patterning of metallic gates can be extended to allow the formation of zero dimensional structures which will be considered later in the context of Coulomb blockade.

## 2. Random telegraph signals

The action of a split-gate constriction as a detector of single electrons can be employed in the study of hopping conduction. If part of the material in the surrounding region is in the hopping regime, the constriction is sensitive to the distribution of electrons amongst the localised states involved in the hopping, and random changes in this distribution produce random telegraph signal (RTS) noise in the constriction's conductance. Mesoscopic hopping conduction is usually studied by looking at reproducible fluctuations in the conductance as a function of gate voltage or magnetic field [4–7], which result from changes in the critical hop. This gives information only on the time-averaged energy levels and mean occupations of the localised states. By looking at a single RTS, each level of which corresponds to a particular electron configuration, we can monitor a hopping process in time and thereby investigate for the first time the detailed properties of an individual hop and the correlations in the motion of electrons caused by Coulomb interactions [8].

Fig. 1 shows the result of sampling the conductance of a single split-gate device at 1 kHz while sweeping the gate voltage  $V_g$  at a temperature of 1.2 K. It is clear that noise appears mainly on the steps between the one-dimensional quantised plateaux, and takes the form of RTSs. The similarity in shape of the curves defined by the two levels of each RTS implies that the conductance modulation is explained by a fairly uniform shift in the potential at the constriction during the RTS transition, the magnitude of which can be deduced from the size of the displacement in  $V_g$  between the two curves and the known rate of change of  $E_F$  with  $V_g$  [9]. In the same device, we isolated an RTS due to hopping conduction by the fact that its characteristics were *time-irreversible* [10], which implied that it was caused by a process occurring out of equilibrium. As there was no dc electric field along the channel, and the ac signal level was not larger than  $k_B T/e$ , the disequilibrium had to be related to current flow along the high electric field between the gate and the 2DEG, even though the gate leakage current could not be resolved with a picoammeter. Fig. 2a shows samples of the RTS at two nearby gate voltages. The time-irreversibility can be seen from the fact that the transition between levels O and A occurs only in the direction  $O \rightarrow A$ , while the reverse,  $A \rightarrow O$ , is never seen. The properties of this RTS are fully consistent with a microscopic model in which the current passes along a chain of two localised states, A and B, with energy levels  $E_A$  and  $E_B$ , whose spatial arrangement is shown in fig. 2b. The four levels of the RTS can be identified with the corresponding charge configurations of these defects as illustrated in fig. 2c. In configuration O both defects are empty, while in configuration AB both are occupied. All observed transitions are shown by arrows. The sequence appropriate to the typical cyclic

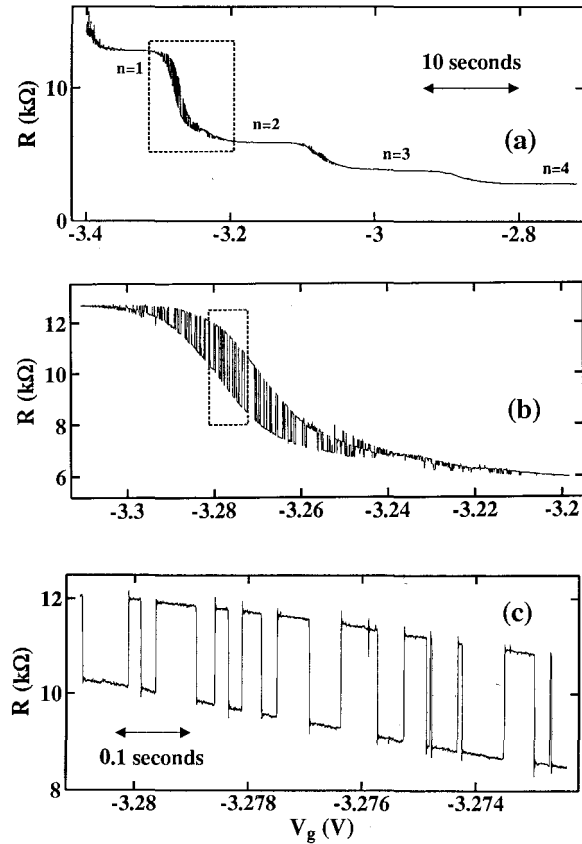


Fig. 1. (b) and (c) are successive magnifications of the gate-voltage sweep shown in (a), for a split-gate device at 1.2 K with the conductance sampled at 1 kHz, showing a large RTS visible between the  $n = 1$  and  $n = 2$  plateaux.

pattern  $O \rightarrow A \rightarrow B \rightarrow O$ , as enclosed in the box on the upper trace of fig. 2a, is emphasised by the thick horizontal arrows, and corresponds to the transfer of a single electron from the gate to the 2DEG.

The distance between the defects and the centre of the constriction in our scheme is of the order of  $1000 \text{ \AA}$ , which is sufficiently large for the potential in this region to be shifted fairly uniformly when the defect charge configuration changes. The potential shifts deduced for this RTS were about  $210 \mu\text{eV}$  for  $O \rightarrow A$  and  $40 \mu\text{eV}$  for  $B \rightarrow O$ . These values are smaller than the unscreened Coulomb potential of an electron at a distance of  $1000 \text{ \AA}$  (about  $1 \text{ meV}$ ), because of the screening effect of the 2DEG. The smaller potential shift associated with defect B is consistent with it being closer to the 2DEG.

The characteristic times of the four-level signal, whose definitions are indicated in fig. 2a, were measured at the two gate voltages  $V'_{g1} = -1.92 \text{ V}$  and

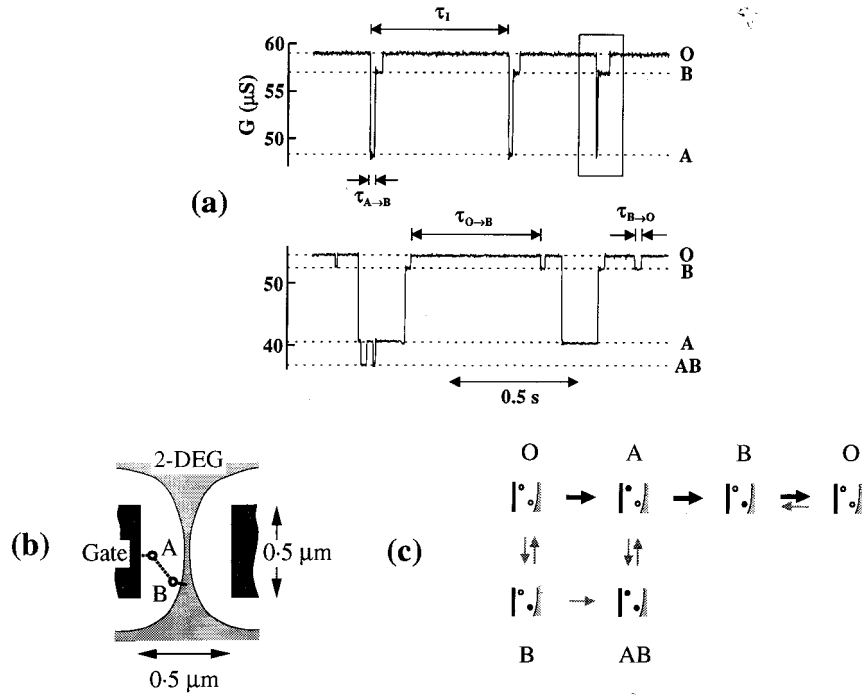


Fig. 2. (a) Samples of an irreversible RTS at  $V_g = -1.91$  V (upper trace) and  $V_g = -1.92$  V (lower trace). (b) Sketch of the geometry of the ballistic constriction in plan view, showing approximate locations of the defects responsible for the irreversible RTS. (c) Diagram indicating observed transitions between electron configurations on the hopping chain between the gate and the 2DEG. The horizontal sequence connected by thick solid arrows corresponds to the portion of the RTS contained within the box in (a).

$V_{g1}'' = -1.96$  V. The current through the chain is given by  $I_{\text{ch}} = e/\tau_1$ , where  $\tau_1$  is the mean time between transitions of the type  $O \rightarrow A$ . At both gate voltages  $\tau_1$  is equal to 1.2 s (giving  $I_{\text{ch}} = 1.3 \times 10^{-19}$  A). This is consistent with transition  $O \rightarrow A$  involving the tunneling of an electron through the Schottky barrier followed by energetic relaxation through the conduction band and subsequent capture by defect A, which is clearly a one-way process. The times  $\tau_{B \rightarrow O} = 10$  ms and  $\tau_{O \rightarrow B} = 2.0$  s are also unchanged from  $V_{g1}'$  to  $V_{g1}''$ , and the detailed-balance requirement  $\exp[-(E_B - E_F)/k_B T] = \tau_{B \rightarrow O}/\tau_{O \rightarrow B}$  yields  $E_B - E_F = 550 \mu\text{eV}$ . The lack of dependence of  $E_B$  on  $V_g$  is explained by the proximity of defect B to 2DEG. In contrast,  $\tau_{A \rightarrow B}$ , the time an electron waits before hopping from A to B, increases from 30 ms at  $V_{g1}'$  to 80 ms at  $V_{g1}''$ . As defect A is considerably closer to the gate,  $E_A$  may be expected to increase faster than  $E_B$  as  $V_g$  is made more negative, and the decrease in the transition rate  $1/\tau_{A \rightarrow B}$  can be explained by a decreasing matrix element for spontaneous phonon emission as  $E_A - E_B$  increases. Using the normal expression  $1/\tau_{A \rightarrow B} \approx \gamma^0 \times$

$\exp(-2r_{AB}/a)$ , where  $a \approx 100 \text{ \AA}$  is the Bohr radius of a donor state and  $\gamma^0 \sim 10^{13} \text{ Hz}$ , we obtain the reasonable estimate of  $1300 \text{ \AA}$  for the separation  $r_{AB}$  of the defects.

It is possible to investigate interaction effects in hopping [8] directly with such a technique of RTS analysis. If the Coulomb interaction between electrons in states A and B were much greater than  $k_B T$  we would expect to find that the probability of transition  $O \rightarrow B$  was much less than that of  $A \rightarrow AB$  – the hopping of electrons into defect B would be blockaded by the presence of an electron in A. However, for the particular RTS discussed here this is not the case, probably because the interaction energy is comparable to that between each defect and the constriction, of order only  $100 \mu\text{eV} \sim k_B T$ . Also, the presence of an electron in B does not inhibit the movement of electrons into A from the gate because of the high-field conditions of this transition.

At more positive  $V_g$  the RTS evolves into a more complicated form which has more levels but in which certain transitions are still irreversible. This is explained by an alteration of the preferred hopping chain to one involving more localised states, by analogy with the alteration of the critical hop which gives rise to fluctuations in the time-averaged hopping conductance.

### 3. Single electron effects

The energy stored on a capacitor with charge  $q$  on one plate and  $-q$  on the other can be worked out using undergraduate physics and comes to  $q^2/2C$ . Moving a single electron from one plate of the capacitor to the other involves an energy  $e^2/C$ . Suppose the dielectric of the capacitor is made very thin so that electrons can tunnel through it. If the capacitance is made very small then this energy can dominate the charge transport and the system shows single electron effects. In particular at low temperatures where the thermal energy  $kT$  is less than  $e^2/2C$ , a voltage  $V$  greater than  $e/2C$  must be applied to get any electrons to tunnel across the barrier separating the two plates of the capacitor. The suppression of tunnelling due to single electron effects is known as the Coulomb blockade. In practice single electron effects exist only where there are small conducting islands separated from connecting leads by tunnel barriers. The capacitance of these islands to the outside world can be as low as  $10^{-17} \text{ F}$ .

The history of this field goes back to the 1960's when it was discovered that the electrical characteristics of small metallic grains sandwiched between thin insulating tunnel barriers change at low temperatures if the grains were made very small (see e.g. Lamb and Jaklevic [11]). The full theory behind this was

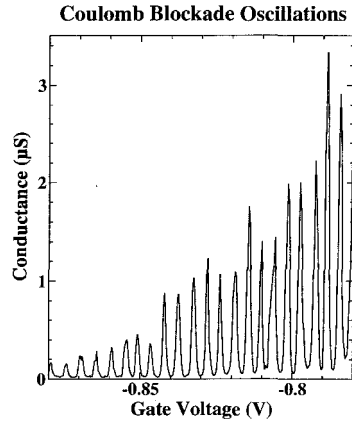


Fig. 3. Coulomb blockade oscillations seen in the conductance as a gate voltage is swept.

not developed until the mid 1980's (Averin and Likharev [12]), which was followed up by many further experiments.

Using semiconductors replaces the metallic grain with a quantum dot in which electrons are confined to a very small region of a semiconductor.

A GaAs/AlGaAs heterostructure is used to confine electrons to a thin sheet at the heterostructure interface. The thin sheet of electrons is called a two dimensional electron gas (2DEG). Metal Schottky gates on the surface are biased negatively to deplete out the electrons in the 2DEG. These gates are patterned using electron beam lithography into shapes that form the outline of a small dot with constrictions to the connecting leads. On applying a negative bias of  $\sim -0.7$  V the only electrons left are in the dot and leads. The constrictions form tunnel barriers between the dot and the leads.

Following the work of Meirav [13], it is found that if the voltage on a gate near one of these quantum dots is varied the conductance oscillates (see fig. 3). This is another manifestation of the charging energy associated with putting a single electron on the dot. The gate used in the above experiment has a small capacitance to the dot, and therefore changing the gate voltage changes the total charging energy of the dot. Adding one electron to the dot from the leads increases the charging energy by  $e^2/C$ . At certain gate voltages the electrons in the leads have sufficient energy to add an electron to the dot, including the  $e^2/C$ . In this case electrons can hop on and off the quantum dot one at a time giving a conductance maximum, while at other gate voltages this is impossible giving a conductance minimum. Sweeping the gate voltage changes the total charging energy continuously and the conductance goes through a sequence of oscillations, each one corresponding to one more (or less depending on

direction) electron on the dot. It is therefore possible to count the number of electrons on the dot.

Finding the potential on a quantum dot island is not easy as one cannot attach a Voltmeter to the dot, since Voltmeters work by exchanging electrons with the object they are measuring, and altering the number of electrons on the dot changes the very thing you are trying to measure. One way round this is to arrange for one of these devices to affect another electrical circuit in close proximity. The electric field associated with the dot will affect the tunnelling resistance of a pinched off split gate next to the dot.

A device that does this is shown in fig. 4 [14]. The large bar down the middle of the picture is biased sufficiently negatively that no electrons can tunnel from one side to the other. This acts to separate two circuits on either side of the bar. To the right of the bar is a quantum dot that shows Coulomb blockade oscillations. The current is passed from top to bottom of the picture and goes through two constrictions defined by split gates. In operation these constrictions form tunnel barriers. The separate gate that makes up the right hand side of the dot can be used to alter the Coulomb charging condition on the dot without changing the heights of the tunnel barriers into or out of the dot. This “plunger” gate is swept to see Coulomb blockade oscillations (see fig. 5a) in the conductance measured across the dot. The second circuit of the left of the vertical bar in the picture is a single split gate. When this is biased in the tunnelling regime (typically at a resistance of  $\sim 100 \text{ k}\Omega$ ) the tunnelling resistance is very sensitive to the local electric field. This circuit acts as a “detector” of the change in potential on the quantum dot, and can sense when an individual electron goes into or out of the dot. This detector can be calibrated directly. Removing the negative potential on the plunger gate on the quantum box opens up the right hand side of the dot. This, of course, destroys the Coulomb blockade since there is no longer any distinct island of electrons. However this does allow a voltage to be applied directly to the 2DEG between the barriers and the effect on the detector to be measured. After calibrating the detector it is possible to work backwards and infer the potential change on the dot from the resistance change of the detector (fig. 5b).

The detector resistance has small dips on a rising background which directly correlate with the CB oscillations in the quantum dot. Using the calibration procedure, the detector resistance can be transformed into the dot potential as shown. The electrostatic potential of the dot,  $\Delta\Phi_{\text{Dot}}$ , is oscillatory with an average amplitude of  $500 \pm 100 \mu\text{V}$  which is therefore the charging energy of the dot. The peaks and troughs of the oscillations in conductance, indicated by the dotted lines, correspond to the mean value of the electrostatic potential oscillations. In a conductance minimum, the Fermi energy in the connecting leads lies approximately midway between the occupied  $N$ th electron state and

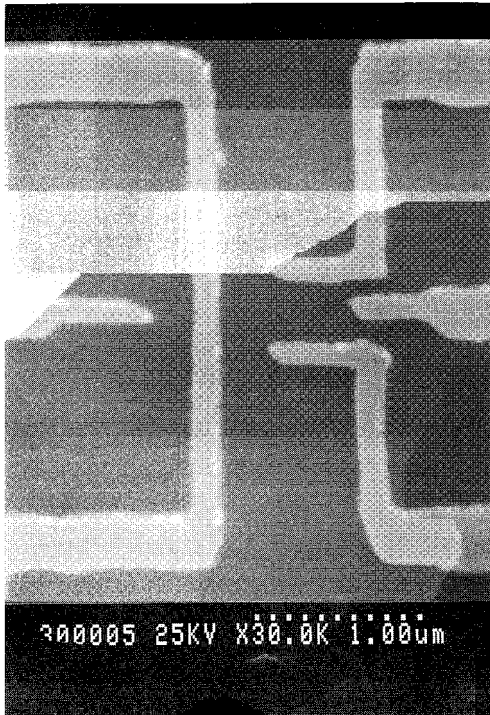


Fig. 4.

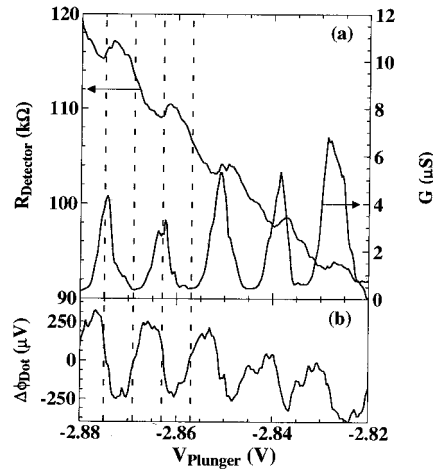


Fig. 5.

Fig. 4. An SEM photograph of a Coulomb blockade device next to a single split gate in a separate detector circuit.

Fig. 5. (a) Coulomb blockade oscillations (as in fig. 3), with the detector resistance superimposed. The detector is picking up the change in potential on the quantum dot. (b) The potential change on the dot as measured by the detector.

the inaccessible  $(N + 1)$ th state (inaccessible because of the required  $e^2/C$  energy to place the electron on the dot). As the voltage on the external gate is made more positive, the energy of the occupied electron states in the dot is reduced with respect to the Fermi energy in the connecting leads, i.e. the potential of the dot becomes more positive. When the  $(N + 1)$ th electron level comes within the energy range of the electrons in the leads, electrons can tunnel in. The electron energy levels in the dot move up and down by the charging energy and the measured average electrostatic potential of the dot becomes more negative reflecting the percentage time an electron is in the dot. The dot potential reflects the difference between the charge on the dot that would minimise the charging energy and the percentage time an extra electron is in the dot. On the conductance peak the dot is occupied 50% of the time by an extra electron and therefore the potential takes the mean value. In between

these positions the percentage occupation by an extra electron either lags or leads the charge required causing the oscillation in potential with plunger voltage. In the case of extremely narrow conductance peaks, this can lead to a sawtooth waveform for the dot potential (see fig. 6).

The charging energy of the dot can also be obtained by measuring the total capacitance of the dot to all other conducting regions around it. CB oscillations have a period in gate voltage of  $e/C_g$ , where  $C_g$  is the capacitance between the gate being swept and the electrons in the dot. With all the gate voltages set as above, sweeping the potential on each gate a small way allows the capacitance between that gate and the dot to be measured directly. In the same way the capacitance of regions of 2DEG separated from the dot by gates can be measured, e.g. applying a bias to the regions of 2DEG between plunger gate and the adjacent gate and observing the CB oscillations. The capacitances of each conducting region are added up to give the total capacitance  $C_\Sigma = 2.92 \pm 0.2 \times 10^{-16}$  F, which implies a potential on the dot due to charging by a single electron  $\Delta\Phi_{\text{Dot}} = e/C_\Sigma = 550 \pm 30 \mu\text{V}$ . This is in good agreement with the value obtained from the detector, especially since the calibration is known to underestimate  $\Delta\Phi_{\text{Dot}}$  slightly.

The tunnel barrier heights were increased until the conductance oscillations were only just measurable. The plunger voltage was then swept negative. The conductance oscillations in the quantum dot die away because the plunger increases the barrier heights, but the signal on the detector remains (see fig. 6). The current through the dot has become too small to be measured, but the detector shows that Coulomb oscillations are still occurring. The oscillations of the detector can be followed for a further 110 periods until the plunger reaches a voltage of  $-4.05$  V, after which the signal vanishes. At this point the current

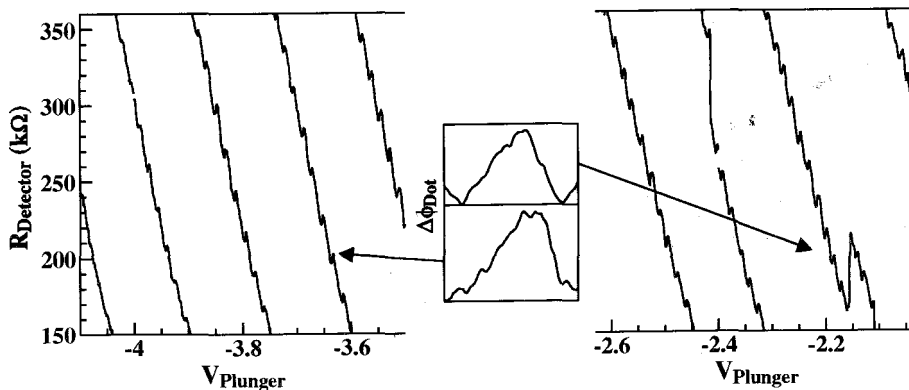


Fig. 6. The Coulomb blockade oscillations have become too small to be measured, but the signal on the detector is still present. Insets: The potential change on the dot at two points. The shape of the potential change has changed from roughly sinusoidal (fig. 5b) to a sawtooth shape.

through the dot is estimated to be  $\sim 10^{-17}$  A, i.e. about 100 electrons per second.

#### 4. Thermoelectric measurements in the Coulomb blockade regime

As discussed above, a patterned gate structure can be used to produce an isolated electron island (or *quantum dot*) separating two reservoirs of 2DEG [15], and if the capacitance  $C$  of this dot is sufficiently small, single electron tunnelling (SET) effects may be observed<sup>#1</sup>. The two most widely studied phenomena are the Coulomb blockade (CB) oscillations in the electrical conductance  $G$  through the dot, as a function of gate voltage, and the Coulomb staircase in the dot's  $I$ - $V$  characteristic. We have already seen how a remote sensor can be used to non-intrusively measure the electrical potential of the dot [14], providing a new method to study these effects. Understanding of the transport mechanisms can also be considerably enhanced by studies of the thermopower  $S$ . When a temperature difference  $\Delta T$  is applied across an electron system, a voltage difference  $\Delta V$  is set up to counteract the flow of electrons, and the ratio between these two quantities is defined as the thermopower, i.e.  $\Delta V = S \Delta T$ . Recent measurements [17] demonstrate Coulomb blockade oscillations in the thermopower of a quantum dot with the same period in gate voltage as those in the conductance. The thermopower is negative when transport through the dot is predominantly by electrons, and positive when hole transport dominates, so that  $S$  oscillates about zero as the gate voltage defining the dot is swept.

A schematic of the device used in these measurements is displayed as an inset in fig. 7. The Schottky gates were used to define a channel of 2DEG, with a split-gate (PC1) on the left, and a quantum dot, produced by PC2 and PC3, on the right. Thermoelectric measurements were made by passing a dc current  $I_{dc}$  along the central channel to increase the electron temperature  $T_e$  in this region above the lattice temperature  $T_L$  [18]. The large regions of 2DEG outside the channel can be assumed to act as electron reservoirs at  $T_L = 550$  mK. The temperature difference,  $\Delta T = (T_e - T_L)$ , between the channel region and the right hand reservoir produces an electrochemical potential difference,  $\Delta\mu_{dot} = -eS_{dot} \Delta T$ , across the quantum dot of thermopower  $S_{dot}$ . The transverse dc voltage,  $V_{tr} = (V_R - V_L)$ , is then equal to  $-\Delta\mu_{dot}/e$  plus a small, constant offset due to the thermopower of PC1 [19].

Fig. 7 displays typical results for the electrical conductance  $G_{dot}$  and transverse voltage  $V_{tr}$  of the quantum dot in the CB regime, as a function of

<sup>#1</sup> For a review of single-electron tunnelling in semiconductor nanostructures, see [16].

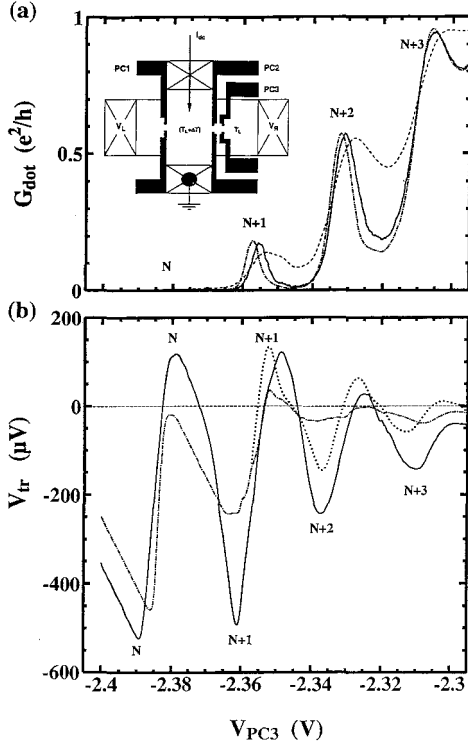


Fig. 7.

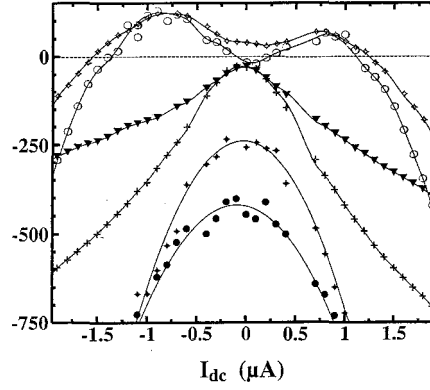


Fig. 8.

Fig. 7. (a)  $G_{\text{dot}}$  as a function of  $V_{\text{PC3}}$  with  $T_L = 550$  mK,  $V_{\text{PC1}} = -2.25$  V,  $V_{\text{PC2}} = -1.65$  V, and at three different heating currents:  $I_{\text{dc}} = 0$  (chained line),  $-0.7$   $\mu\text{A}$  (solid), and  $2.0$   $\mu\text{A}$  (dashed). The peaks are marked with the inferred number of electrons in the dot:  $N$ ,  $N+1$ , etc. Inset: Schematic of the device, showing the three split-gates (black) used to define the heating channel and quantum dot. (b)  $V_{\text{tr}}$  measured as a function of  $V_{\text{PC3}}$  for the conditions described above, with  $I_{\text{dc}} = 0$  (chained line) and  $-0.7$   $\mu\text{A}$  (solid); and the theoretical prediction (dotted) for  $V_{\text{tr}}$  at  $|I_{\text{dc}}| = 0.7$   $\mu\text{A}$ , calculated as outlined in the text.

Fig. 8. Extrema of  $V_{\text{tr}}$  plotted as a function of  $I_{\text{dc}}$  under the same conditions as fig. 1, for the maxima  $N$  ( $\circ$ ) and  $N+1$  ( $\diamond$ ); and the minima  $N$  ( $\bullet$ ),  $N+1$  ( $\blacklozenge$ ),  $N+2$  ( $+$ ) and  $N+3$  ( $\blacktriangledown$ ). The lines are purely a guide for the eye.

gate voltage on PC3 ( $V_{\text{PC3}}$ ). For  $V_{\text{PC3}} < -2.25$  V transmission was by tunnelling ( $G_{\text{dot}} < 2e^2/h$ ). In this regime, oscillations in  $G_{\text{dot}}$  were observed as a function of both  $V_{\text{PC2}}$  and  $V_{\text{PC3}}$  (fig. 7a). These oscillations were superimposed upon a rapidly rising background. From additional dc bias experiments [17] we were able to determine a value of  $e^2/C \approx 2.5$  meV for the charging energy of the dot. This value is consistent with the observation that an ac voltage of 2 mV destroyed the CB oscillations, and that small amplitude oscillations were still present at  $T_L = 4.2$  K. The transverse voltage  $V_{\text{tr}}$  is plotted as a function of  $V_{\text{PC3}}$  in fig. 7b. For  $I_{\text{dc}} = -0.7$   $\mu\text{A}$ ,  $V_{\text{tr}}$  shows large oscillations in  $V_{\text{PC3}}$  with the same

period as the CB oscillations in  $G_{\text{dot}}$ . The amplitude of these oscillations was found to increase with  $|I_{\text{dc}}|$ , as expected for a thermoelectric voltage, which should be proportional to  $\Delta T$ . When no deliberate temperature difference was applied ( $I_{\text{dc}} = 0$ ), a background gate-voltage dependence was still observed (chained line in fig. 1b), which we attribute to unintentional noise heating in the sample, but this background was generally much smaller than the measured signal.

In fig. 8 the maxima and minima of  $V_{\text{tr}}$  are plotted as a function of  $I_{\text{dc}}$ , showing  $V_{\text{tr}}$  to be a predominantly even function of  $I_{\text{dc}}$ . This is expected for a thermoelectric voltage which depends on  $\Delta T$  through  $|I_{\text{dc}}|$  only. As the gates were biased with respect to one end of the central channel, an asymmetry with respect to the direction of  $I_{\text{dc}}$  is introduced, which is probably responsible for the small asymmetry in fig. 8 (typically less than 30%). For  $|I_{\text{dc}}| < 0.5 \mu\text{A}$  the maxima (minima) in  $V_{\text{tr}}$  increase (decrease) with  $|I_{\text{dc}}|$ , consistent with  $S_{\text{dot}} > 0$  ( $S_{\text{dot}} < 0$ ), and so the amplitude increases with  $\Delta T$ . As the heating current is increased beyond  $|I_{\text{dc}}| = 0.5 \mu\text{A}$ , the maxima saturate and, for  $|I_{\text{dc}}| > 1.5 \mu\text{A}$ ,  $V_{\text{tr}}$  is everywhere negative. In this regime,  $T_e$  is so large that electrons will be thermally excited over the electrostatic barriers defining the quantum dot. Activated transport by electrons always results in a negative thermopower [20]. The high proportion of activation also destroys the minima in  $G_{\text{dot}}$ , as we see in fig. 7a for  $I_{\text{dc}} = 2 \mu\text{A}$ .

We now consider a simple derivation of the thermopower of a quantum dot which separates a left-hand reservoir of temperature  $(T + \Delta T)$  and electrochemical potential  $\mu_{\text{L}}$ , from a right-hand reservoir of temperature  $T$  and electrochemical potential  $\mu_{\text{R}} = \mu_{\text{L}} - e\Delta V_{\text{th}}$ , where  $\Delta V_{\text{th}}$  is the thermoelectric voltage created by the temperature difference,  $\Delta T$ . In the regime of Coulomb charging we define  $\varepsilon_N$  to be the highest occupied energy-level of a dot containing  $N$  electrons. The addition of an extra electron to the dot raises this energy by  $e^2/C$ , to  $\varepsilon_{N+1} = \varepsilon_N + e^2/C$ . For the situation depicted in fig. 9,  $\varepsilon_{N+1}$  is the closest Coulomb level to  $\mu_{\text{L}}$ , but the ground state of the system is the  $N$ -electron configuration. Electrons can only tunnel into the dot if they are thermally activated above the energy  $\varepsilon_{N+1}$ , so that the effective transmission function  $t_e(\varepsilon)$  for electrons through the dot is a step-function in energy, as depicted in fig. 9b. When  $\varepsilon_{N+1} - \mu_{\text{L}} \gg k_{\text{B}}T$  the electrical conductance falls exponentially to zero, however, there is still a small Boltzmann tail of electrons at energy  $\varepsilon_{N+1}$  which are capable of tunnelling into the dot. The thermopower is measured when zero current flows, so we must equate the number of electrons at  $\varepsilon_{N+1}$  in the two reservoirs, given by  $f_{\text{L}}(\varepsilon_{N+1}) = \exp[-(\varepsilon_{N+1} - \mu_{\text{L}})/k_{\text{B}}(T + \Delta T)]$  and  $f_{\text{R}}(\varepsilon_{N+1}) = \exp[-(\varepsilon_{N+1} - \mu_{\text{L}} - e\Delta V)/k_{\text{B}}T]$ . This gives a value for the thermopower,  $S \equiv -\Delta V/\Delta T = -(k_{\text{B}}/e)[(\varepsilon_{N+1} - \mu_{\text{L}})/k_{\text{B}}T]$ , which is a standard result for activated electron transport [20]. Note that  $S < 0$ .

When  $\varepsilon_N$  is the closest Coulomb level to the Fermi energy (see fig. 9c),

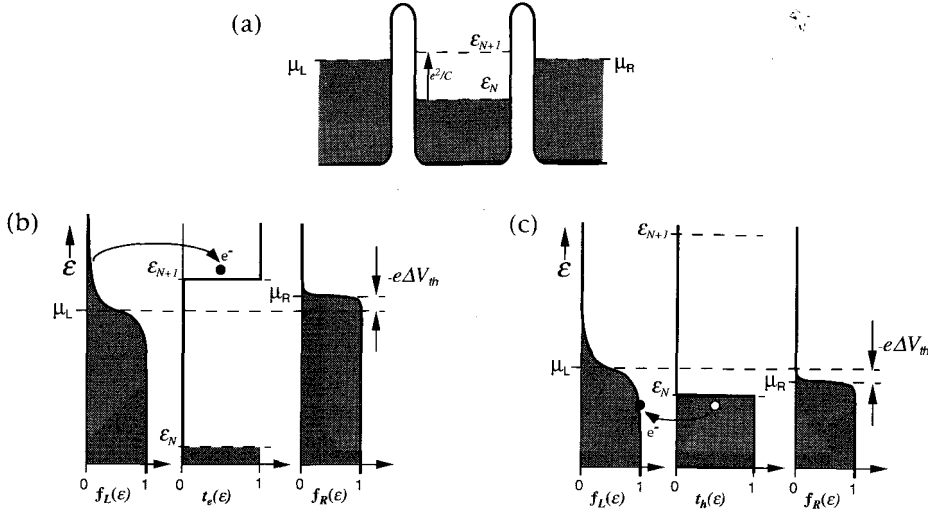


Fig. 9. (a) Energy diagram for an electron island separating two electron reservoirs, with a charging energy on the island of  $e^2/C$ . Here the energy  $\epsilon_N$  represents the maximum electron energy in the  $N$ -electron ground state of the system. (b) When  $\epsilon_{N+1}$  is the closest Coulomb level to the main Fermi energy of the system, electron transport can only occur at  $\epsilon > \epsilon_{N+1}$ , where  $t(\epsilon) = 1$ . Because  $T_L > T_R$ , there are more electrons able to tunnel from left-to-right than in the reverse direction. To maintain current balance,  $\mu_R$  must rise, resulting in a negative thermopower. (c) When  $\epsilon_N$  is the closest level, electrons can tunnel from the dot into available states in the reservoirs. Because of its higher temperature, the left-hand reservoir has more holes below  $\mu$  than that on the right-hand side. To maintain current balance,  $\mu_R$  must decrease, this time giving a positive thermopower.

transport is due to thermally activated holes tunnelling into the dot, below the energy  $\epsilon_N$ . The above argument again applies, except that now  $S = (k_B/e)[(\mu_L - \epsilon_N)/k_B T]$ , and the thermopower is positive. As the gate voltage defining the dot is swept, the thermopower reaches an absolute minimum of  $-e/2CT$  when  $\epsilon_{N+1}$  is  $e^2/2C$  above  $E_F$ , and then abruptly changes to a maximum of  $+e/2CT$  as the nearest available transport level changes to  $\epsilon_N$ , which is  $e^2/2C$  below  $E_F$ , resulting in a saw-tooth lineshape as a function of  $E_F$  (or gate voltage). This saw-tooth lineshape was recently predicted by a more detailed theory [21].

The above argument applies only if the transmission functions are perfect step-functions in energy. If there is any co-tunnelling present these may be spread in energy by an amount greater than  $k_B T$ , allowing for metallic transport near the Fermi energy. In this case we would expect the standard result for thermopower in metallic systems, first derived by Mott and Jones [22], which states the thermopower is proportional to the energy derivative of the electrical conductance. We have calculated this for the data in fig. 7, by taking the derivative of  $G_{\text{dot}}$  with respect to gate voltage, and hence, energy.

The calculated result is the dotted line in fig. 7b, which shows good agreement with the experimental data. Here  $\Delta T = 1.2$  K, which was obtained from additional measurements on one of the 1D ballistic constrictions (PC2), and fitting the results to predictions for a saddle-shaped potential [23]. We also compared our data with that expected for fully activated transport. Not only did we fail to observe the predicted sawtooth lineshape, but the amplitude of the experimental thermopower oscillations was an order of magnitude smaller than the theoretical value of  $e/CT$ .

In summary, we have observed CB oscillations in the thermopower of a quantum dot using a current heating technique. The voltage across the dot, which was approximately even in the applied heating current, was used as a measure of the thermopower. Our data showed reasonable agreement with that predicted for metallic transport, and we attribute this metallic behaviour to the presence of broadening.

### Acknowledgement

This work was supported by the U.K. Science and Engineering Research Council.

### References

- [1] D.A. Wharam, T.J. Thornton, R. Newbury, M. Pepper, H. Ahmed, J.E.F. Frost, D.G. Hasko, D.C. Peacock, D.A. Ritchie and G.A.C. Jones, *J. Phys. C* 21 (1988) L209.
- [2] B.J. van Wees, H. van Houten, C.W. Beenakker, J.G. Williamson, L.P. Kouwenhoven, D. van der Mard and C.T. Foxon, *Phys. Rev. Lett.* 60 (1988) 848.
- [3] N.K. Patel, J.T. Nicholls, L. Martin-Moreno, M. Pepper, J.E.F. Frost, D.A. Ritchie and G.A.C. Jones, *Phys. Rev. B* 44 (1991) 13549.
- [4] A.B. Fowler, A. Hartstein and R.A. Webb, *Phys. Rev. Lett.* 48 (1982) 196.
- [5] R.F.K. Kwasnick, M.A. Kastner, J. Melngailis and P.A. Lee, *Phys. Rev. Lett.* 52 (1984) 224.
- [6] A.O. Orlov and A.K. Savchenko, *JETP Lett.* 47 (1988) 470.
- [7] R.J. Stroh and M. Pepper, *J. Phys. Cond. Matt.* 1 (1989) 8481.
- [8] K.S. Chase and D.J. Thouless, *Phys. Rev. B* 39 (1989) 1989.
- [9] D.H. Cobden, N.K. Patel, M. Pepper, D.A. Ritchie, J.E.F. Frost and G.A.C. Jones, *Phys. Rev. B* 44 (1991) 1938.
- [10] D.H. Cobden, A.K. Savchenko, M. Pepper, N.K. Patel, D.A. Ritchie, J.E.F. Frost and G.A.C. Jones, *Phys. Rev. Lett.* 69 (1992) 502.
- [11] J. Lambe and R.C. Jaklevic, *Phys. Rev. Lett.* 22 (1969) 1371.
- [12] D.V. Averin and K.K. Likharev, *Quantum Effects in Small Disordered Systems*, B. Al'tshuler, P.A. Lee and R.A. Webb, eds. (Elsevier, Amsterdam, 1991).
- [13] U. Meirav, M.A. Kastner, S.J. Wind, *Phys. Rev. Lett.* 65 (1990) 771.

- [14] M. Field, C.G. Smith, M. Pepper, D.A. Ritchie, J.E.F. Frost, G.A.C. Jones and D.G. Hasko, *Phys. Rev. Lett.* 70 (1993) 1311.
- [15] C.G. Smith, M. Pepper, R. Newbury, H. Ahmed, J.E.F. Frost, D.G. Hasko, D.C. Peacock, D.A. Ritchie and G.A.C. Jones, *J. Phys. C* 21 (1988) L893.
- [16] H. van Houten, C.W.J. Beenakker and A.A.M. Staring, in: *Single Charge Tunnelling*, H. Grabert and M.H. Devoret, eds., vol. 294, NATO Advanced Study Institute, Series B: Physics (Plenum, New York, 1992) p. 167.
- [17] A.S. Dzurak, C.G. Smith, M. Pepper, D.A. Ritchie, J.E.F. Frost, G.A.C. Jones and D.G. Hasko, *Solid State Commun.*, to be published.
- [18] A.P. Long and M. Pepper, *Physica B* 117 (1983) 75;  
R.T. Syme, M.J. Kelly and M. Pepper, *J. Phys. C* 1 (1989) 3375.
- [19] L.W. Molenkamp, H. van Houten, C.W.J. Beenakker, R. Eppenga and C.T. Foxon, *Phys. Rev. Lett.* 65 (1990) 1052.
- [20] M. Cutler and N.F. Mott, *Phys. Rev.* 181 (1969) 1336.
- [21] C.W.J. Beenakker and A.A.M. Staring, *Phys. Rev. B* 46 (1992) 9667.
- [22] N.F. Mott and H. Jones, *The Theory and Properties of Metals and Alloys* (Clarendon, Oxford, 1936).
- [23] A.S. Dzurak, C.G. Smith, L. Martin-Moreno, M. Pepper, D.A. Ritchie, G.A.C. Jones and D.G. Hasko, *J. Phys.: Condens. Matter*, to be published.